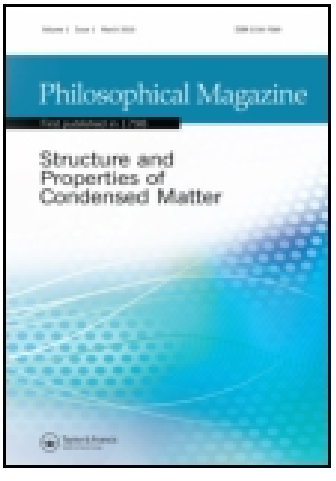

Philosophical Magazine
Publication details, including instructions for authors and subscription information:
http://www.tandfonline.com/loi/tphm20

Evaluation of dislocation energy in thin films

R.A. Coppeta[a], D. Holec[b], H. Ceric[c] & T. Grasser[a]

[a] Institute for Microelectronics, Technische Universität Wien, A-1040 Wien, Austria.

[b] Department of Physical Metallurgy and Materials Testing, Montanuniversität Leoben, A-8700 Leoben, Austria.

[c] Christian Doppler Laboratory for Reliability Issues in Microelectronics at the Institute for Microelectronics, Technische Universität Wien, A-1040 Wien, Austria.

To cite this article: R.A. Coppeta, D. Holec, H. Ceric & T. Grasser (2015) Evaluation of dislocation energy in thin films, Philosophical Magazine, 95:2, 186-209, DOI: 10.1080/14786435.2014.994573

To link to this article: http://dx.doi.org/10.1080/14786435.2014.994573

Philosophical Magazine, 2015
Vol. 95, No. 2, 186–209, http://dx.doi.org/10.1080/14786435.2014.994573

Evaluation of dislocation energy in thin films

R.A. Coppeta[a]*, D. Holec[b], H. Ceric[c] and T. Grasser[a]

[a] *Institute for Microelectronics, Technische Universität Wien, A-1040 Wien, Austria;* [b] *Department of Physical Metallurgy and Materials Testing, Montanuniversität Leoben, A-8700 Leoben, Austria;* [c] *Christian Doppler Laboratory for Reliability Issues in Microelectronics at the Institute for Microelectronics, Technische Universität Wien, A-1040 Wien, Austria*

(*Received 29 August 2014; accepted 26 November 2014*)

A procedure is proposed to calculate the energy of a misfit dislocation at the interface of a film with a finite thickness and a substrate with semi-infinite thickness when modelled anisotropically and with different elastic properties. The results are compared with the treatments derived by Steeds, Willis, Jain and Bullough, and Freund. The new formula is used to calculate the equilibrium critical thickness for $Al_xGa_{1-x}N$/GaN, $In_xGa_{1-x}N$/GaN and $Si_{1-x}Ge_x$/Si heterostructures. A comparison with experimental data from the literature shows good agreement. In contrast to other models, application of the new formula for dislocation energy yields smaller critical thickness for the onset of the misfit dislocations.

Keywords: dislocations; critical thickness; heterostructure

1. Introduction

A serious issue for the reliability and performance of heterostructure devices is the deteriorating impact of dislocations, mostly originating from epitaxy, when a thin layer is grown on a substrate with significantly different lattice parameters. Below a certain layer thickness, called the *critical thickness* (CT), the layer is grown pseudomorphically on a substrate, i.e. the layer is grown with the same lattice parameter as the substrate. Consequently, the layer is strained, leading to large strain energy. When CT is reached, a relaxation of the strain occurs via plastic flow. The most common mechanism of plastic relaxation is the introduction of misfit dislocations (MDs) along the interface between the film and the substrate.

Several models have been proposed to calculate CT. In 1974, Matthews and Blakeslee [1] compared the force exerted by strain on the extension of the MD line with the tension in the dislocation line acting against its elongation. Their model assumes that both the film and the substrate have the same isotropic elastic properties, the film has a finite thickness (however, neglecting the free surface effects) and the substrate is semi-infinite. Starting from the same hypotheses, Freund [2,3] compared the energy necessary to create a MD with the energy inside the fully strained thin film. He arrived at the same CT formula as Matthews and Blakeslee. However, the two models differ conceptually:

*Corresponding author. Email: coppeta@iue.tuwien.ac.at

Matthews and Blakeslee assumed a pre-existing dislocation in the substrate which creates an MD segment along the heteroepitaxial interface due to the action of the misfit stress; Freund assumed a freshly generated dislocation at the film surface which glides into the interface between the film and the substrate. The impact of the free surface of the film and the difference between the elastic constants of the film and the substrate on the CT was discussed by Willis, Jain and Bullough [4], yet they still worked in the framework of isotropic elasticity.

The anisotropy of the heterostructure can be considered in the CT calculation using the methodology developed by Steeds [5] for the energy of an infinitely long straight dislocation inside an anisotropic medium. This has been done in the works by Holec et al. [6–8], however, the free surfaces and differences in elastic response of the film and the substrate were ignored.

In this paper, we close the gap by evaluating the impact of different effects – elastic anisotropy, difference between the elastic constants of the film and the substrate, the free surface of the film – on CT values. After reviewing the methodology, we apply it to several material systems, namely, $Al_xGa_{1-x}N$/GaN, $In_xGa_{1-x}N$/GaN, and $Si_{1-x}Ge_x$/Si, and compare with available experimental data from literature. We also calculate the pre-logarithmic factors related to the dislocation core structure using analytical continuum models. These compare favourably with values obtained through atomistic simulations available in the literature.

2. The critical thickness criterion

The system shown in Figure 1 is composed of a thin film with a finite thickness in the region $0 < z < h$, and a semi-infinite substrate filling the half-space $z < 0$. The critical thickness criterion compares the dislocation energy per unit length, $\mathcal{E}$, with the work, $\mathcal{W}$, done by the misfit stress, σ^m_{ij}, during the bringing of the unit length of a dislocation from the film surface into the film–substrate interface. As a consequence, the CT criterion is given by

$$\mathcal{W} = \mathcal{E}. \tag{1}$$

2.1. *Work done by the misfit strain*

Since the film is much thinner than the semi-infinite substrate, the strain in the substrate is assumed to be zero, while the complete lattice mismatch is accommodated in the film (i.e. we neglect any mismatch strain relaxation by substrate bending). According to the geometry shown in Figure 1, the top surface $z = h$ of the film is traction free and therefore $\sigma^m_{xz}(x, h) = \sigma^m_{zz}(x, h) = \sigma^m_{yz}(x, h) = 0$. Assuming that all directions within the xy-plane (the hexagonal plane) are equivalent, a planar stress state is obtained and thus the mismatch strain components are $\varepsilon^m_{xx} = \varepsilon^m_{yy} = \varepsilon_m$, where ε_m is the misfit strain, defined as

$$\varepsilon_m = \frac{a^* - a}{a}, \tag{2}$$

considering that the thin film's in-plane lattice constant a adjusts to the rigid substrate's lattice constant a^*.

Hooke's law for isotropic structures reads

$$\begin{pmatrix}\sigma_{xx}\\ \sigma_{yy}\\ \sigma_{zz}\\ \sigma_{yz}\\ \sigma_{xz}\\ \sigma_{xy}\end{pmatrix}=\begin{pmatrix}C_{11} & C_{12} & C_{12} & 0 & 0 & 0\\ C_{12} & C_{11} & C_{12} & 0 & 0 & 0\\ C_{12} & C_{12} & C_{11} & 0 & 0 & 0\\ 0 & 0 & 0 & C_{44} & 0 & 0\\ 0 & 0 & 0 & 0 & C_{44} & 0\\ 0 & 0 & 0 & 0 & 0 & C_{44}\end{pmatrix}\begin{pmatrix}\varepsilon_{xx}\\ \varepsilon_{yy}\\ \varepsilon_{zz}\\ 2\varepsilon_{yz}\\ 2\varepsilon_{xz}\\ 2\varepsilon_{xy}\end{pmatrix}, \tag{3}$$

where $C_{44} = (C_{11} - C_{12})/2$. In the case of cubic and hexagonal symmetries, the shape of the stiffness matrix C_{ij} changes to

$$\begin{pmatrix}C_{11} & C_{12} & C_{12} & 0 & 0 & 0\\ C_{12} & C_{11} & C_{12} & 0 & 0 & 0\\ C_{12} & C_{12} & C_{11} & 0 & 0 & 0\\ 0 & 0 & 0 & C_{44} & 0 & 0\\ 0 & 0 & 0 & 0 & C_{44} & 0\\ 0 & 0 & 0 & 0 & 0 & C_{44}\end{pmatrix}, \quad \text{and} \quad \begin{pmatrix}C_{11} & C_{12} & C_{13} & 0 & 0 & 0\\ C_{12} & C_{11} & C_{13} & 0 & 0 & 0\\ C_{13} & C_{13} & C_{33} & 0 & 0 & 0\\ 0 & 0 & 0 & C_{44} & 0 & 0\\ 0 & 0 & 0 & 0 & C_{44} & 0\\ 0 & 0 & 0 & 0 & 0 & C_{66}\end{pmatrix}, \tag{4}$$

respectively, where $C_{66} = (C_{11} - C_{12})/2$ for the hexagonal symmetry (the right matrix above).

Considering, for example, the hexagonal symmetry, Hooke's law gives

$$0 = \sigma_{zz}^m = C_{13}\varepsilon_{xx}^m + C_{13}\varepsilon_{yy}^m + C_{33}\varepsilon_{zz}^m \tag{5}$$

which results in

$$\varepsilon_{zz}^m = -2\frac{C_{13}}{C_{33}}\varepsilon_m. \tag{6}$$

Finally, Hooke's law yields for the mismatch stress

$$\sigma_m = \sigma_{xx}^m = \sigma_{yy}^m = \frac{(C_{11} + C_{12})C_{33} - 2C_{13}^2}{C_{33}}\varepsilon_m. \tag{7}$$

In the chosen Cartesian coordinate system, the Burgers vector $\mathbf{b}$, the tensor of the misfit stress $\boldsymbol{\sigma}_m$ and the outer normal to the cut surface $\Gamma = S_2 + S_4$ (see Figure 2) denoted by $\mathbf{n}$ take the forms

$$\mathbf{b} = \begin{pmatrix}-b\sin\theta\sin\phi\\ b\cos\theta\\ b\sin\theta\cos\phi\end{pmatrix}, \quad \boldsymbol{\sigma}_{\mathrm{m}} = \begin{pmatrix}\sigma_m & 0 & 0\\ 0 & \sigma_m & 0\\ 0 & 0 & 0\end{pmatrix}, \quad \mathbf{n} = \begin{pmatrix}-\cos\phi\\ 0\\ \sin\phi\end{pmatrix}, \tag{8}$$

where θ is the angle between the dislocation line and the Burgers vector, and ϕ the angle between the slip plane and the normal to the film–substrate interface (see Figure 1). The *work per unit length of the dislocation*, $\mathcal{W}$, done by the misfit stress is calculated according to [3]

$$\mathcal{W} = \int_0^{h/\cos\phi} \sum_{i,j} b_i \sigma_{ij}^m n_j \, dz = \int_0^{h/\cos\phi} \sum_i \left(b_i\sigma_{ix}n_x + b_i\sigma_{iz}n_z\right) dz = b\sigma_m h \sin\theta\sin\phi. \tag{9}$$

In a straightforward manner, analogous expressions for the other symmetries of the stiffness tensor (isotropic or cubic) can also be obtained.

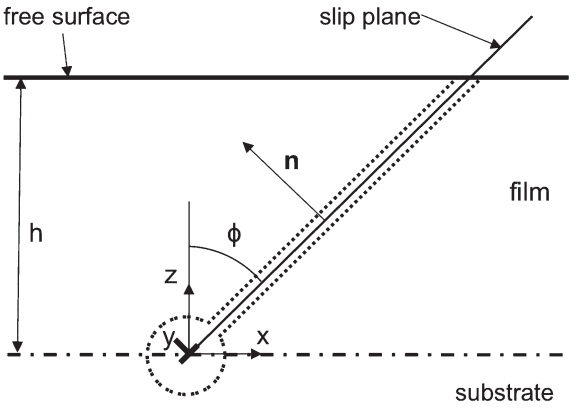

Figure 1. The straight infinitely long dislocation at the film–substrate interface. The film thickness is h, the slip plane is tilted by an angle ϕ from the normal to the interface.

2.2. *Dislocation energy*

The linear elasticity theory provides the framework to derive the dislocation energy. This theory breaks down in the dislocation core region, therefore, an inner cut-off parameter r_c is conveniently introduced to separate the dislocation core (plastic region) from the elastic region. r_c is usually taken to be $b/2$, where b is the length of the Burgers vector [3].

The subsequent treatment is developed for the simplified geometry shown in Figure 2. The *energy per unit length of the dislocation* $\mathcal{E}$ (for simplicity often called just the dislocation energy) may be divided into two parts:

$$\mathcal{E} = \mathcal{E}_{\text{core}} + \mathcal{E}_{\text{d}}, \tag{10}$$

where $\mathcal{E}_{\text{core}}$ and $\mathcal{E}_{\text{d}}$ account for energy inside and outside the dislocation core region, respectively. For large film thickness h (see Figure 2), the core energy constitutes only a minor contribution to the total dislocation energy and is thus neglected in the following calculation. Let $\boldsymbol{\sigma^d}$ be the stress tensor associated with the strain field $\boldsymbol{\epsilon^d}$ caused by the straight dislocation. Then the strain energy of the dislocation is given by

$$\mathcal{E}_{\text{d}} = \tfrac{1}{2}\int_V \sum_{ij} \sigma_{ij}^d \epsilon_{ij}^d \,\mathrm{d}V = \tfrac{1}{2}\sum_{ij}\int_V \tfrac{1}{2}\left(\frac{\partial u_i}{\partial x_j} + \frac{\partial u_j}{\partial x_i}\right)\sigma_{ij}^d \,\mathrm{d}V \tag{11}$$

using the symmetry of the stress tensor $\sigma_{ij}^d = \sigma_{ji}^d$

$$\tfrac{1}{2}\sum_{ij}\int_V \frac{\partial u_i}{\partial x_j}\sigma_{ij}^d \,\mathrm{d}V = \tfrac{1}{2}\sum_{ij}\int_V \frac{\partial}{\partial x_j}\left(u_i\sigma_{ij}^d\right)\mathrm{d}V - \tfrac{1}{2}\sum_{ij}\int_V u_i\frac{\partial \sigma_{ij}^d}{\partial x_j}\,\mathrm{d}V. \tag{12}$$

Recalling the equilibrium conditions for elastic media,

$$\sum_j \frac{\partial \sigma_{ij}^d}{\partial x_j} = 0, \tag{13}$$

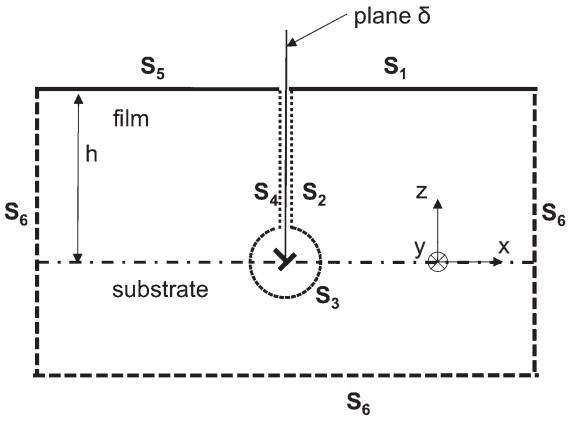

Figure 2. The dislocation is formed by an offset (defined by the Burgers vector **b**) of one side S_4 of the plane δ with respect to the other side S_2. The surface S_3 encloses the dislocation core region. h denotes the film thickness.

we obtain

$$\mathcal{E}_{\mathrm{d}} = \tfrac{1}{2} \sum_{ij} \int_V \frac{\partial}{\partial x_j} \left(u_i \sigma_{ij}^d \right) \mathrm{d}V. \tag{14}$$

Using the Gauss–Ostrogradsky theorem to transform the volume integral into a surface integral over the surface S enclosing the volume V:

$$\tfrac{1}{2} \sum_{ij} \int_V \frac{\partial}{\partial x_j} \left(u_i \sigma_{ij}^d \right) \mathrm{d}V = \tfrac{1}{2} \sum_{ij} \int_S u_i \sigma_{ij}^d n_j \, \mathrm{d}S \tag{15}$$

The surface S can be divided into five parts (see Figure 2) and the last equation can be rewritten as

$$\tfrac{1}{2} \sum_{k=1}^{5} \left(\sum_{ij} \int_{S_k} u_i \sigma_{ij}^d n_j \, \mathrm{d}S_k \right). \tag{16}$$

Along the free surface (S_1 and S_5) of the film, $\sigma_{zz} = \sigma_{xz} = \sigma_{yz} = 0$ and $\boldsymbol{n} = (0, 0, 1)$, so

$$\int_{S_1} u_i \sigma_{ij}^d n_j \, \mathrm{d}S_1 = \int_{S_5} u_i \sigma_{ij}^d n_j \, \mathrm{d}S_5 = 0. \tag{17}$$

Since S_6 is supposed to be infinitely far from the dislocation, the displacements vanish and the contribution of the surface is zero.

The surface S_3 is a cylindrical surface whose axis is aligned along the y-axis. Since the dislocation is infinite along the y direction, $\boldsymbol{n} = (n_x, 0, n_z)$:

$$\tfrac{1}{2} \sum_{ij} \int_{S_3} u_i \sigma_{ij}^d n_j \, \mathrm{d}S_3 = \tfrac{1}{2} \sum_{i} \int_{S_3} \left(u_i \sigma_{ix}^d n_x + u_i \sigma_{iz}^d n_z \right) \mathrm{d}S_3 \tag{18}$$

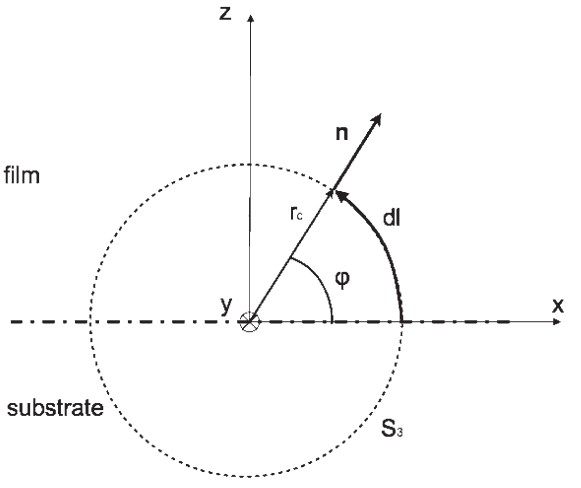

Figure 3. The core surface S_3 in a cylindrical coordinate system.

To simplify the integration, it is convenient to transform the Cartesian coordinates into the cylindrical coordinates (see Figure 3) as

$$\begin{aligned} x &= r_{\mathrm{c}} \cos\varphi, \\ y &= t\ , \\ z &= r_{\mathrm{c}} \sin\varphi. \end{aligned} \tag{19}$$

Consequently,

$$\mathrm{d}S_3 = \mathrm{d}l\mathrm{d}y = r_{\mathrm{c}}\mathrm{d}\varphi\mathrm{d}y. \tag{20}$$

Considering that $\boldsymbol{n} = (\cos\varphi, 0, \sin\varphi)$, Equation (18) per unit length along y becomes

$$\tfrac{1}{2}\int_0^{2\pi} \sum_i u_i \left(\sigma_{ix}^d \cos\varphi + \sigma_{iz}^d \sin\varphi\right) r_{\mathrm{c}}\, \mathrm{d}\varphi, \qquad i = x,\ y,\ z. \tag{21}$$

Expanding the last equation yields

$$\tfrac{1}{2} r_{\mathrm{c}} \int_0^{2\pi} \left(\underbrace{u_x \left(\sigma_{xx}^d \cos\varphi + \sigma_{xz}^d \sin\varphi\right)}_{\text{edge}} + \underbrace{u_y \left(\sigma_{yx}^d \cos\varphi + \sigma_{yz}^d \sin\varphi\right)}_{\text{screw}} + \underbrace{u_z \left(\sigma_{zx}^d \cos\varphi + \sigma_{zz}^d \sin\varphi\right)}_{\text{edge}} \right) \mathrm{d}\varphi. \tag{22}$$

The substitution of the displacements and the stress components expressed in cylindrical coordinates allows for the evaluation of the impact of the core surface on the dislocation energy.

When the impact of the core integral along S_3 is negligible, only the integrals along surfaces S_2 and S_4 have to be considered. The evaluation of these two integrals for a straight dislocation inside an infinite isotropic medium yields the classic formula for the dislocation energy [3,9,10]:

$$\mathcal{E}_{\mathrm{d}} = \frac{\mu b^2 \left(1 - \nu \cos^2\theta\right)}{4\pi \left(1 - \nu\right)} \ln\left(\frac{R}{r_{\mathrm{c}}}\right), \tag{23}$$

where μ and ν are the shear modulus and the Poisson ratio, respectively, θ is the angle between the Burgers vector **b** and the dislocation line, and R is the outer cut-off radius. Here, we take it to be equal to the film thickness.

If the straight dislocation is considered inside an infinite anisotropic medium, the evaluation of the integrals along the surfaces S_2 and S_4 yields the formula derived by Steeds [5]:

$$\mathcal{E}_{\mathrm{d}} = \tfrac{1}{4\pi} \sum_{ij} \mathrm{K}_{ij} b_i b_j \ln\left(\frac{R}{r_{\mathrm{c}}}\right), \tag{24}$$

where K_{ij} is called energy factor and it is a function of the crystal structure and the elastic properties.

If the evaluation of the integrals along the surfaces S_2 and S_4 is performed for a straight dislocation at the interface between a finite isotropic film and an semi-infinite isotropic substrate with different elastic constants, the formula developed by Willis et al. [4] is obtained.

In this paper, the evaluation (see Appendix 1) of the integrals along the surfaces S_2 and S_4 is performed for the most general case, e.g. for a straight dislocation at the interface between a finite anisotropic film and a semi-infinite anisotropic substrate with different elastic constants:

$$\mathcal{E}_{\mathrm{d}} = \tfrac{1}{2} \int_{r_c}^{h} \sum_{ij} b_i \sigma_{ij} n_j \mathrm{d}z. \tag{25}$$

In conclusion, four approaches (summarized in Table 1) for calculating the dislocation energy were defined above, which will be used to evaluate the impact of different approximations.

2.3. *The CT models*

According to Equation (1), equating the work done by the misfit strain with each of the four formulas for dislocation energy yields four different models with which to calculate the equilibrium CT. These models are reported with the respective hypotheses in Table 1 and their results are discussed in the subsequent paragraphs. In particular, the CT model developed by Freund [2], which neglects the differences between film and substrate, considers only isotropic elasticity, and in its simplified (often used) formula, also neglects the effect of the free surface, is indicated by F. The F model corrected for the elastic anisotropy using the Steeds formula for the dislocation energy [5] is denoted by S. The fully isotropic model, but with the free surface and different elastic constants in the film and the substrate, employs the Willis, Jain and Bullough formula [4], and is indicated by WJB. Finally, a model addressing all effects as described in Appendix 1 is named S+WJB.

3. Impact of the anisotropy on the CT criterion

Steeds in his book [5] developed a procedure to calculate the energy of one infinite straight dislocation in the bulk of an infinite material considered anisotropic with a certain crystallographic symmetry. The result for the hexagonal symmetry is briefly described in [6].

Table 1. An overview of different assumptions for evaluating misfit dislocation energy, and equilibrium CT.

	Freund (F) [2,3]	Steeds (S) [5]	Willis et al. (WJB) [4]	Steeds + Willis et al. (S+WJB) Appendix 1
Anisotropy	no	yes	no	yes
Different elastic properties of the film and the substrate	no	no	yes	yes
Free surface of the film	no	no	yes	yes

Here, we adopt this treatment in order to calculate the energy (with and without the contribution of the dislocation core) for a dislocation whose slip system is $1/3\langle 1\,1\,\bar{2}\,3\rangle\{1\,1\,\bar{2}\,2\}$ or $1/3\langle 1\,1\,\bar{2}\,3\rangle\{1\,\bar{1}\,0\,1\}$ in $Al_{0.2}Ga_{0.8}N$ and in $In_{0.2}Ga_{0.8}N$. The same treatment with the appropriate elastic constants is used to calculate the energy for the so-called 60° dislocation slip system $\langle 1\,1\,0\rangle\{1\,1\,1\}$ in $Si_{0.8}Ge_{0.2}$. The used material constants are listed in Appendix 2.

In the following, we discuss the difference between the dislocation energy $\mathcal{E}_d$ and the work $\mathcal{W}$ done by the misfit stress field for each alloy. When the resulting value is positive, fully coherent accommodation of the misfit strain is energetically preferred, while for negative values, the introduction of misfit dislocations becomes favoured. The highest film thickness yielding the difference of 0 indicates the equilibrium CT.

The resulting values for the three different alloys as a function of the film thickness are plotted in Figures 4–6. Each figure has two sets of curves, one for the F (isotropic elasticity) and one for the S (anisotropic elasticity) procedures. For all systems investigated here, the anisotropy lowers CT. Additionally, it turns out that the inclusion of the integral along the core surface S_3 (values labelled "with E_{cs}" in the figures) has, in all cases, only a negligible impact (or at least on order of magnitude smaller effect than the correct crystal symmetry) on the predicted CT (see Table 2).

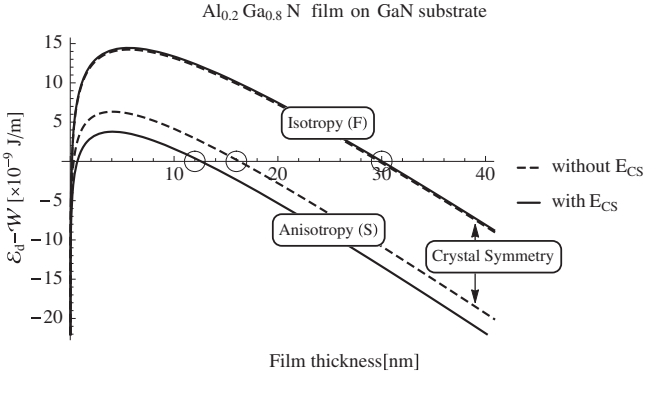

Figure 4. $\mathcal{E}_d - \mathcal{W}$ as function of the film thickness. $\mathcal{E}_d$ is calculated assuming isotropic (F) and anisotropic (S) elasticity, with or without the evaluation of the integral along the core surface E_{cs}. $\mathcal{W}$ is calculated according to Equation (9). The CTs are indicated by a circle.

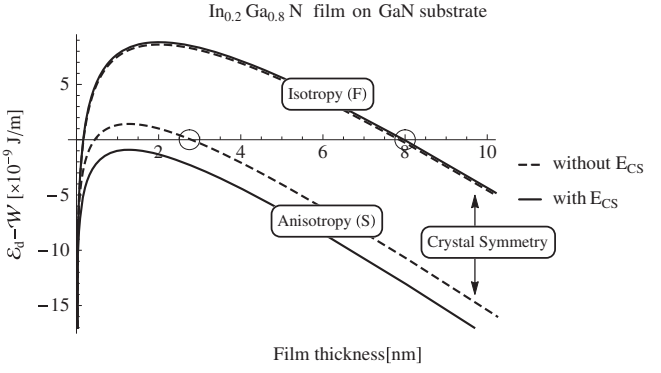

Figure 5. $\mathcal{E}_d - \mathcal{W}$ as function of the film thickness. $\mathcal{E}_d$ is calculated assuming isotropic (F) and anisotropic (S) elasticity, with or without the evaluation of the integral along the core surface E_{cs}. $\mathcal{W}$ is calculated according to Equation (9). The CTs are indicated by a circle.

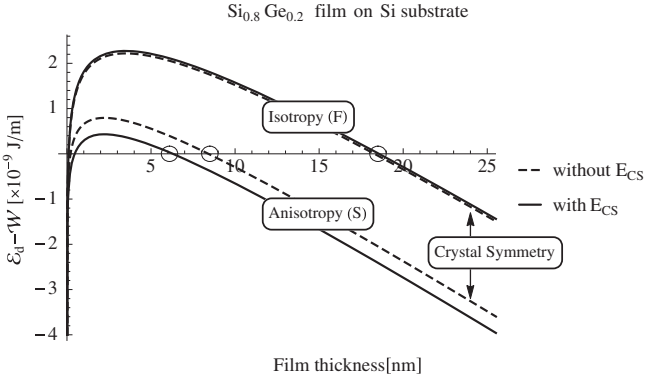

Figure 6. $\mathcal{E}_d - \mathcal{W}$ as function of the film thickness. $\mathcal{E}_d$ is calculated assuming isotropic (F) and anisotropic (S) elasticity, with or without the evaluation of the integral along the core surface E_{cs}. $\mathcal{W}$ is calculated according to Equation (9). The CTs are indicated by a circle.

Table 2. CT values (in nm) of the studied systems.

	F	F+E_{cs}	S	S+E_{cs}	WJB	S+WJB
$Al_{0.2}Ga_{0.8}N$ film on GaN substrate	30	30	16	12	93	17
$In_{0.2}Ga_{0.8}N$ film on GaN substrate	8	8	3	0	26	5
$Si_{0.2}Ge_{0.8}$ film on Si substrate	18	18	8	6	74	16

4. The critical thickness according to WJB

Willis et al. [4] derived a procedure to evaluate the integrals along the S_2 and S_4 surfaces in order to calculate the energy $\mathcal{E}_d$ of a misfit dislocation at the interface between a film with a finite thickness and a semi-infinite substrate. The film and the substrate are both supposed

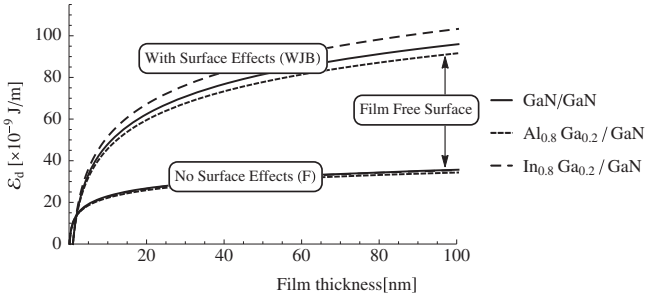

Figure 7. $\mathcal{E}_d$ is function of the film thickness for $Al_xGa_{1-x}N$/GaN and $In_xGa_{1-x}N$/GaN systems. The $\langle 11\bar{2}3\rangle\{1\ \bar{1}\ 0\ 1\}$ slip system is considered. The two sets of curves are calculated through the WJB and F procedures, respectively.

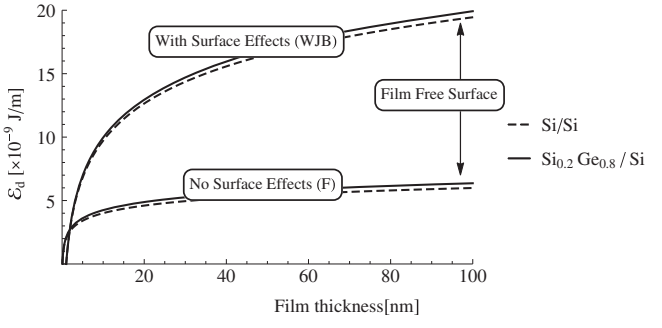

Figure 8. $\mathcal{E}_d$ is function of the film thickness for $Si_{1-x}Ge_x$/Si. The $\langle 1\ 1\ 0\rangle\{1\ 1\ 1\}$ slip system of a 60° dislocation is considered. The two sets of curves are calculated through the WJB and F procedures, respectively.

to be isotropic but with different elastic properties. Figure 7 shows two sets of curves representing $\mathcal{E}_d$ as a function of the film thickness for three different systems: $Al_{0.2}Ga_{0.8}N$ film on GaN substrate, $In_{0.2}Ga_{0.8}N$ on GaN and a GaN film grown on GaN substrate. One set of the $\mathcal{E}_d$ curves is calculated adopting the WJB model, while the second uses the F treatment. Therefore, the difference stems from including (WJB) or neglecting (F) the free surface effects and the difference in the elastic constants of the film and the substrate. In both cases, the isotropic elasticity framework is used. The curves within each set are very close to each other, meaning that the impact of different elastic properties of the film and the substrate is negligible. Therefore, it can be concluded that the difference between the two sets originates predominantly from the impact of free surface. This factor significantly increases the $\mathcal{E}_d$ term and, as a consequence, also the CT value. Figure 8 shows a similar analysis for two different systems: a $Si_{0.2}Ge_{0.8}$ film on a Si substrate and a Si film grown on a Si substrate. As in the case of the III-nitrides, the variation caused by the different elastic properties of the film and the substrate is negligible. On the other hand, the difference between the WJB and F formalism, which is now related predominantly to the inclusion of the free surface, is significant. Therefore, also for silicon, the free surface increases $\mathcal{E}_d$ and, as a consequence, the CT value.

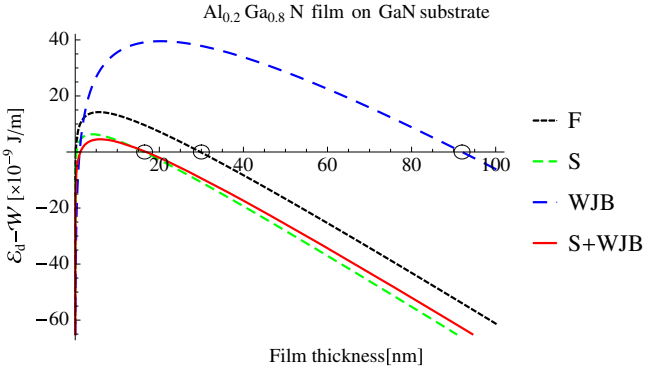

Figure 9. (colour online) $\mathcal{E}_d - \mathcal{W}$ is function of the film thickness. $\mathcal{E}_d$ is calculated according to F, S, WJB and S+WJB approaches. $\mathcal{W}$ is calculated according to Equation (9). The CTs are indicated by a circle.

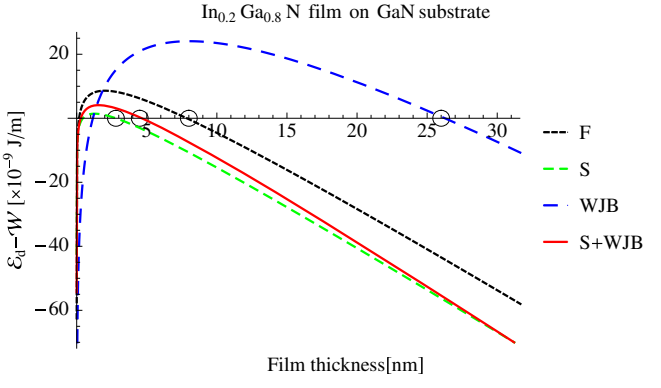

Figure 10. (colour online) $\mathcal{E}_d - \mathcal{W}$ is a function of the film thickness. $\mathcal{E}_d$ is calculated according to F, S, WJB and S+WJB approaches. $\mathcal{W}$ is calculated according to Equation (9). The CTs are indicated by a circle.

5. Overall comparison of various effects on predicted critical thickness

In order to consider the anisotropy, the difference between the elastic properties of the film and the substrate and the impact of the free surface, we combine the S and the WJB approaches. Based on the conclusions of Section 3, in the following, we neglected the contribution of the integral along the core surface S_3. The detailed mathematical derivation of this treatment (indicated with S+WJB) is given in Appendix 1. The model S+WJB is used to compute $\mathcal{E}_d$ as a function of the film thickness for three different alloys: a $Al_{0.2}Ga_{0.8}N$ film on a GaN substrate, $In_{0.2}Ga_{0.8}N$ on GaN and a $Si_{0.8}Ge_{0.2}$ film on a Si substrate. The results are shown and compared with corresponding F, S and WJB results in Figures 9–11. The CT values of the systems are listed in Table 2. Considering all the three systems, the WJB model increases CT by ≈300% with respect to the F model. The CT value of the theoretically most complete scheme, S+WJB, is always between the S and the F values. In particular, the S+WJB CT is lower by ≈50% relative to the F CT for $Al_{0.2}Ga_{0.8}N$ and $In_{0.2}Ga_{0.8}N$, while it is the same in the case of $Si_{0.8}Ge_{0.2}$.

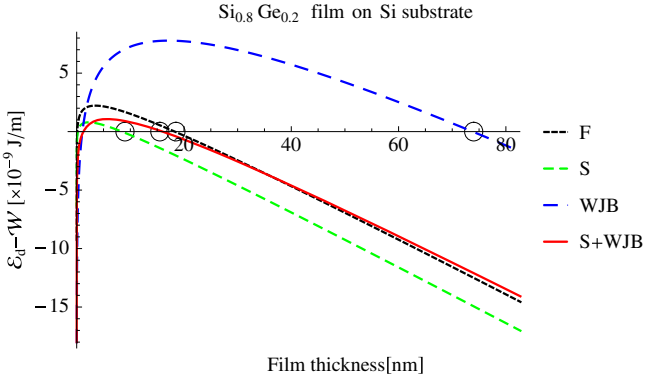

Figure 11. (colour online) $\mathcal{E}_d - \mathcal{W}$ is a function of the film thickness. $\mathcal{E}_d$ is calculated according to F, S, WJB and S+WJB approaches. $\mathcal{W}$ is calculated according to Equation (9). The CTs are indicated by a circle.

6. Comparison of pre-logarithmic terms based on a continuum and atomistic approach

$\mathcal{E}_d$ is a logarithmic function of the film thickness

$$\mathcal{E}_d \approx c \ \log h. \tag{26}$$

The continuum approach allows for the extraction of the pre-logarithmic coefficient c for each alloy considered in this work. The validity of continuum elasticity results for treating the dislocation energy outside the core region has been demonstrated by an atomic-scale computer simulation [10]. These simulations allow for the calculation of the strain energy $\mathcal{E}_d$ within a cylinder of radius R with the dislocation along its axis. $\mathcal{E}_d$ varies logarithmically with R for $R \geq r_c$, where r_c is the core radius. For $R < r_c$, the logarithmic behaviour is lost due to the singularity along the dislocation line. In Table 3, the pre-logarithmic coefficients predicted using the F (dislocation in infinitely large uniform isotropic medium) and S (dislocation in infinitely large uniform anisotropic medium) are summarized, and compared with values obtained from atomistic simulations [11–14]. In general, good agreement is found between the S model and the atomistic simulations whenever the data are available in the literature. This result is understandable as the atomistic simulations consider a dislocation in an infinite anisotropic structure, which is the same assumption of the S model.

To express the total energy of a dislocation (Equation (10)), the dislocation core energy needs to be added to the continuum formula for the bulk energy. Based on the above comparison, the continuum approach, including the elastic anisotropy, seems to be compatible with the atomistic evaluation of the dislocation core energy and radius. Since this information is available only for certain compositions, we calculated the dislocation core energy for each composition of the alloys through linear interpolation (Vegard-like behaviour) of the values summarized in Table 4. For example, in the case of $Si_{1-x}Ge_x$, one gets

$$\mathcal{E}_{\text{core}}\Big|_{Si_{1-x}Ge_x} = x\mathcal{E}_{\text{core}}\Big|_{Ge} + (1-x)\mathcal{E}_{\text{core}}\Big|_{Si}. \tag{27}$$

Table 3. Pre-logarithmic terms for different alloys according to the F (isotropic) and S (anisotropic) models evaluated in this paper. Data from atomistic simulations are included whenever available.

material	Si	$Si_{0.5}Ge_{0.5}$	$In_{0.2}Ga_{0.8}N$	$Al_{0.2}Ga_{0.8}N$	GaN
unit of measure	$\times 10^{-9}$ J/m	$\times 10^{-9}$ J/m	$\times 10^{-9}$ J/m	$\times 10^{-9}$ J/m	$\times 10^{-9}$ J/m
dislocation	60° dislocation	60° dislocation	$\langle 1\,1\,\bar{2}\,3\rangle\{1\bar{1}01\}$	$\langle 11\bar{2}3\rangle\{1\bar{1}01\}$	(a+c)-type
F	1.7	1.7	5.55	5.44	5.51
S	0.56	0.52	3.53	3.95	3.94
atomistic simulation		0.64 [11]			3.44 [13]

Table 4. Parameters of the dislocation cores from atomistic simulations. 0.43 eV/Å is equal to 0.64 nJ/m.

material	dislocation	$\mathcal{E}_{core}$ [eV/Å]	Prelogarithmic term [eV/Å]	Reference
Si	60°	0.43		[12]
$Si_{0.5}Ge_{0.5}$	60°	0.59	0.43	[11]
GaN	(a+c)-type	3.12	2.15	[13]
GaN	a-type	1.61	0.81	[14]
AlN	a-type	1.71	0.90	[14]
InN	a-type	1.66	0.41	[14]

The core energy $\mathcal{E}_{core}$ for Ge was calculated by linearly extrapolating the core energies of Si and $Si_{0.5}Ge_{0.5}$. Analogous expressions were also used for $Al_xGa_{1-x}N$ and $In_xGa_{1-x}N$.

7. Comparison between theoretical and experimental CT

After illustrating the differences among various treatments of dislocation energy, and their impact on the equilibrium CT, we use the F and S+WJB models, including the dislocation core energies estimated in the last paragraph, to calculate the equilibrium CT as a function of composition, x, for the three different alloys. The two models, F and S+WJB, are chosen as they are based on opposite hypotheses (see Table 1).

We considered the $1/3\langle 1\,1\,\bar{2}\,3\rangle\{1\,\bar{1}\,0\,1\}$ and $1/3\langle 1\,1\,\bar{2}\,3\rangle\{1\,1\,\bar{2}\,2\}$ slip systems for $Al_xGa_{1-x}N$/GaN and $In_xGa_{1-x}N$/GaN, and the 60° misfit dislocation with the $\langle 1\,1\,0\rangle\{1\,1\,1\}$ slip system for $Si_{1-x}Ge_x$/Si. The calculated CT results obtained from the F and S + WJB models are compared with experimental observations and data available in literature (Figures 12–14).

The difference between the F and S+WJB results is small, with the S+WJB model yielding lower values when compared to F. In all cases, the experimental data are close to the theoretical curves, suggesting that the experimental CT values were obtained from epitaxial depositions close to the thermodynamical equilibrium.

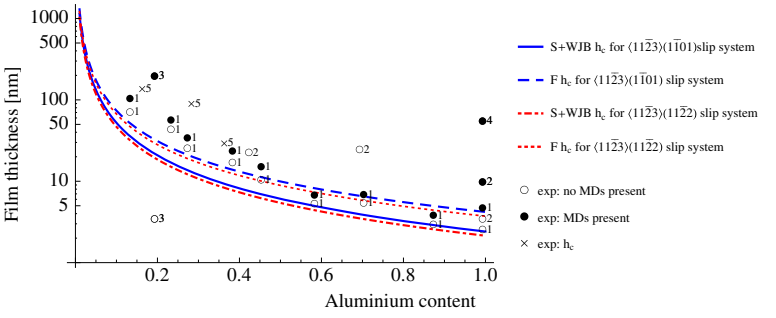

Figure 12. (colour online) The equilibrium CT as a function of the AlN mole fraction x calculated through F and S+WJB models including the core energy. The theoretical curves are compared with experimental data, 1-[15], 2-[16], 3-[17], 4-[18], 5-[19].

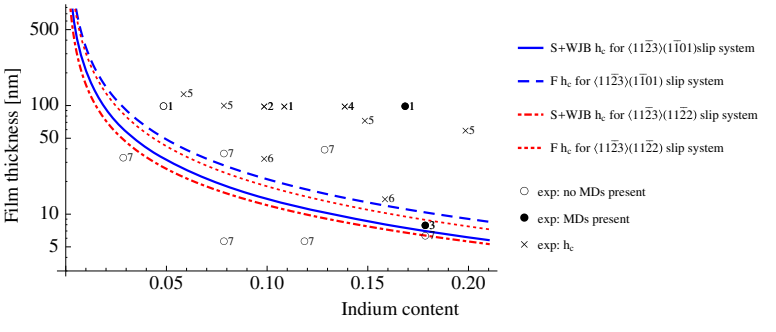

Figure 13. (colour online) The equilibrium CT as a function of the InN mole fraction x calculated through F and S+WJB models including the core energy. The theoretical curves are compared with experimental data, 1-[20], 2-[21], 3-[22], 4-[23], 5-[24], 6-[25], 7-[6].

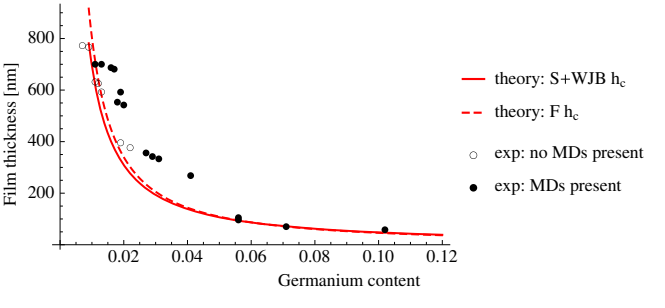

Figure 14. (colour online) The equilibrium CT as a function of the Ge fraction x calculated through F (dashed line) and S+WJB (solid line) models including the core energy. The 60° misfit dislocation with the ⟨1 1 0⟩{1 1 1} slip system is considered. The theoretical curves are compared with experimental data from [26].

Regarding the $Al_xGa_{1-x}N$/GaN and $In_xGa_{1-x}N$/GaN systems, the S+WJB model provides a more severe condition for the onset of the MD at the interface than the F model. It is important to realize that the here reported CT is the so-called *equilibrium* CT. This means that it corresponds to the configuration where it, for the first time, becomes energetically favourable to relieve the misfit strain by introducing MDs. However, any mechanism for the creation of the MDs, which may require certain extra activation energy, is not considered in the model. Similarly, parameters influencing kinetics of the epitaxial deposition, such as temperature and deposition rate, are also not considered by the equilibrium CT models. Finally, the current experiment techniques are unable to detect the exact onset of the appearance of MDs. It, therefore, follows that no MDs are expected *below* the predicted CT values, however, the detection of MDs may be (sometimes significantly) higher than the equilibrium CT.

A closer inspection of Figures 12–14 reveals that the here refined S+WJB model fulfils this criterion (unlike the F model).

8. Conclusions

We have revisited the different continuum-based approaches for calculating the energy of a straight infinitely long dislocation in an elastic medium. Motivated by the misfit dislocations in a heteroepitaxial interface, we have evaluated separately the influence of (i) free surface, (ii) different elastic constants in the film and substrate and (iii) elastic anisotropy. Our results suggest that starting from a homogeneous infinite isotropic medium, the inclusion of a free surface increases the dislocation energy, and the difference in elastic constants of the film and substrate does not play any significant role (because it is typically an order of magnitude smaller than the impact of, e.g. the free surface), while the inclusion of elastic anisotropy decreases the dislocation energy.

In order to include the dislocation core energy in the evaluation of the equilibrium critical thickness, we compared the pre-logarithmic terms of the analytical models with the corresponding values obtained by atomistic simulations. We found a good agreement between the continuum predictions based on anisotropic elasticity.

Finally, equilibrium CT was calculated for three important heteroepitaxial material systems, namely $Al_xGa_{1-x}N$/GaN, $In_xGa_{1-x}N$/GaN and $Si_{1-x}Ge_x$/Si. We have proposed a model including elastic anisotropy of the film and the substrate, the difference of their elastic constants and the impact of the film free surface. Recalling that this is a model for equilibrium CT, i.e. it provides a condition when it first becomes energetically favourable to start the relaxation of the mismatch strain via plastic flow, our refined model yields an excellent agreement with the available experimental data in the sense that no MDs are detected below the here predicted threshold.

Funding

This work was jointly funded by the Austrian Research Promotion Agency (FFG, Project No. 831163) and the Carinthian Economic Promotion Fund (KWF, contract KWF-15212274134186).

References

[1] J.W. Matthews and A.E. Blakeslee, J. Cryst. Growth 27 (1974) p.118.
[2] L.B. Freund, J. Appl. Mech. 54 (1987) p.554.

[3] L.B. Freund and S. Suresh, *Thin Film Materials*, Cambridge University Press, Cambridge, 2003.
[4] J.R. Willis, S. Jain and R. Bullough, Philos. Mag. A. A 62 (1990) p.115.
[5] J.W. Steeds, *Introduction to Anisotropic Elasticity Theory of Dislocations*, Clarendon Press, Oxford, 1973.
[6] D. Holec, Y. Zhang, D.V.S. Rao, M. Kappers, C.J. McAleese and C.J. Humphreys, J. Appl. Phys. 104 (2008) p.123514.
[7] D. Holec and C.J. Humphreys, Mater. Sci. Forum 567–568 (2008) p.209.
[8] D. Holec, P.M.F.J. Costa, M.J. Kappers and C.J. Humphreys, J. Cryst. Growth 303 (2007) p.314.
[9] J.P. Hirth and J. Lothe, *Theory of Dislocations*, Krieger Publishing Company, Malabar, FL, 1982.
[10] D. Hull and D.J. Bacon, *Introduction to Dislocations*, Butterworth-Heinemann, Oxford, 2011.
[11] I.N. Remediakis, D.J. Jesson and P.C. Kelires, Phys. Rev. Lett. 97 (2006) p.255502.
[12] L. Gen, M. Qing-yuan, Y. Li-jun and L. Cheng-xiang, J. Atom. Molec. Phys. (2006) p.71.
[13] I. Belabbas, A. Bere, J. Chen, S. Petit, M.A. Belkhir, P. Ruterana and G. Nouet, Phys. Rev. B: Condens. Matter 75 (2007) p.115201.
[14] J. Kioseoglou, P. Komninou and T. Karakostas, Phys. Status Solidi A 206 (2009) p.1931.
[15] S.R. Lee, D.D. Koleske, K.C. Cross, J.A. Floro, K.E. Waldrip, A.T. Wise and S. Mahajan, J. Appl. Phys. 85 (2004) p.6164.
[16] P. Vennéguès, Z. Bougrioua, J.M. Bethoux, M. Azize and O. Tottereau, J. Appl. Phys. 97 (2005) p.024912.
[17] J.-M. Bethoux and P. Venngus, J. Appl. Phys. 97 (2005) p.123504.
[18] M. Gherasimova, G. Cui, Z. Ren, J. Su, X.-L. Wang, J. Han, K. Higashimine and N. Otsuka, J. Appl. Phys. 95 (2004) p.2921.
[19] J.A. Floro, D.M. Follstaedt, P. Provencio, S.J. Hearne and S.R. Lee, Appl. Phys. Lett. 94 (2003) p.1565.
[20] R. Liu, J. Mei, S. Srinivasan, F.A. Ponce, H. Omiya, Y. Narukawa and T. Mukai, Appl. Phys. Lett. 89 (2006) p.201911.
[21] S. Srinivasan, L. Geng, R. Liu, F.A. Ponce, Y. Narukawa, S. Tanaka, Appl. Phys. Lett. 83 (2003) p.5187.
[22] W. Lü, D.B. Li, C.R. Li and Z. Zhang, J. Appl. Phys. 96 (2004) p.5267.
[23] B. Jahnen, M. Albrecht, W. Dorsch, S. Christiansen, H.P. Strunk, D. Hanser and R.F. Davis, MRS Internet J. Nitride Semicond. Res. 3 (1998) p.39.
[24] C.A. Parker, J.C. Roberts, S.M. Bedair, M.J. Reed, S.X. Liu and N.A. El-Masry, Appl. Phys. Lett. 75 (1999) p.2776.
[25] M.J. Reed and N.A. El-Masry, Appl. Phys. Lett. 77 (2000) p.4121.
[26] D.C. Houghton, C.J. Gibbings, C.G. Tuppen, M.H. Lyons and M.A.G. Halliwell, Appl. Phys. Lett. 56 (1990) p.460.
[27] R.R. Reeber and K. Wang, MRS Internet J. Nitride Semicond. Res. 6 (2001) p.1.
[28] M.A. Hopcroft, W. Nix and T. Kenny, J. Microelectromech. S. 19 (2010) p.229.
[29] H. Morkoc, *Handbook of Nitride – Semiconductors and Devices*, Vol. 1, WILEY-VCH Verlag, Darmstadt, 2008.

Appendix 1. A straight dislocation at the interface of anisotropic materials

The evaluation of the integrals along the surfaces S_2 and S_4 (see Figure 2) deals with a straight dislocation at the interface between a finite anisotropic film and a semi-infinite anisotropic substrate with different elastic properties:

$$\mathcal{E}_{\mathrm{d}} = \tfrac{1}{2} \sum_{ij} \left(\int_{S_2} u_i \sigma_{ij}^d n_j \, \mathrm{d}S_2 + \int_{S_4} u_i \sigma_{ij}^d n_j \, \mathrm{d}S_4 \right) \tag{A1}$$

Considering Figure A1, the previous equation becomes

$$\frac{1}{2}\sum_i \left(\int_{r_c}^{h} u_i \left(x \to 0^+\right) \sigma_{ix}^d \, \mathrm{d}z + \int_{h}^{r_c} u_i (x \to 0^-) \sigma_{ix}^d \, \mathrm{d}z \right). \tag{A2}$$

If the extremes of the second integral are inverted, one obtains

$$\mathcal{E}_\mathrm{d} = \frac{1}{2}\sum_i \int_{r_c}^{h} b_i \sigma_{ix}^d \, \mathrm{d}z \tag{A3}$$

where $u_i(x \to 0^+) - u_i(x \to 0^-) = b_i$.

The evaluation of the stress components in (A3) is performed through the treatment of the Willis, Jain and Bullough model [4] for the hexagonal and cubic symmetries following the Steeds procedure [5].

The dislocation of interest is a misfit dislocation along the c-plane of the wurtzite structure or the closed-packed plane of the diamond structure. The z-axis is perpendicular to the c-plane or to the closed-packed plane, respectively (see Figure A2). The dislocation is considered straight and extended to infinite along the y-axis. This assumption simplifies the problem to a plane strain problem where no quantity depends on the y-coordinate, so

$$\frac{\partial}{\partial y} = 0, \tag{A4}$$

The Burgers vector of the dislocation is **b**. Displacements are given by the functions u_x, u_y and u_z. The displacements u_x and u_z correspond to the edge component of the considered dislocation, whereas u_y corresponds to the screw component. Strain components are

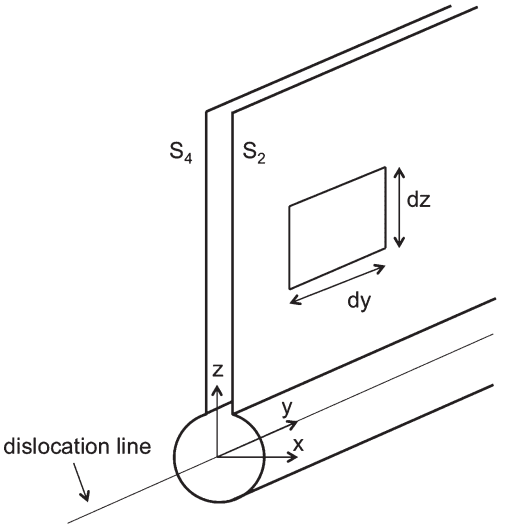

Figure A1. The z-axis is perpendicular to the c-plane for the hexagonal symmetry and to the closed-packed plane for the cubic one. The dislocation line lies along the y-axis in both cases.

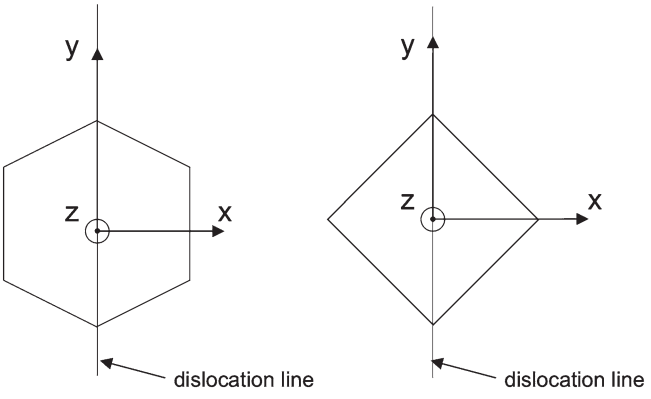

Figure A2. The z-axis is perpendicular to the c-plane for the hexagonal symmetry and to the closed-packed plane for the cubic one. The dislocation line lies along the y-axis in both cases.

$$\begin{aligned} \varepsilon_{xx} &= \frac{\partial u_x}{\partial x}, \quad & \varepsilon_{xy} &= \frac{1}{2}\frac{\partial u_y}{\partial x}, \\ \varepsilon_{yy} &= 0, & \varepsilon_{xz} &= \frac{1}{2}\left(\frac{\partial u_x}{\partial z} + \frac{\partial u_z}{\partial x}\right), \\ \varepsilon_{zz} &= \frac{\partial u_z}{\partial z}, & \varepsilon_{yz} &= \frac{1}{2}\frac{\partial u_y}{\partial z}. \end{aligned} \tag{A5}$$

The compatibility Equations [5] provides two relations:

$$\frac{\partial^2 \varepsilon_{xx}}{\partial z^2} + \frac{\partial^2 \varepsilon_{zz}}{\partial x^2} = 2\frac{\partial \varepsilon_{xz}}{\partial x \partial z}, \tag{A6a}$$

$$\frac{\partial \varepsilon_{yz}}{\partial x} - \frac{\partial \varepsilon_{xy}}{\partial z} = 0. \tag{A6b}$$

The fact that $\varepsilon_{yy} = 0$ yields a relation between particular stress components:

$$0 = \varepsilon_{yy} = S_{12}\sigma_{xx} + S_{11}\sigma_{yy} + S_{13}\sigma_{zz} \quad \Rightarrow \quad \sigma_{yy} = -\frac{S_{12}}{S_{11}}\sigma_{xx} - \frac{S_{13}}{S_{11}}\sigma_{zz}. \tag{A7}$$

The compliances reflecting the proper hexagonal symmetry have been used:

$$\begin{pmatrix} \varepsilon_{xx} \\ \varepsilon_{yy} \\ \varepsilon_{zz} \\ 2\varepsilon_{yz} \\ 2\varepsilon_{xz} \\ 2\varepsilon_{xy} \end{pmatrix} = \begin{pmatrix} S_{11} & S_{12} & S_{13} & 0 & 0 & 0 \\ S_{12} & S_{11} & S_{13} & 0 & 0 & 0 \\ S_{13} & S_{13} & S_{33} & 0 & 0 & 0 \\ 0 & 0 & 0 & S_{44} & 0 & 0 \\ 0 & 0 & 0 & 0 & S_{44} & 0 \\ 0 & 0 & 0 & 0 & 0 & S_{66} \end{pmatrix} \begin{pmatrix} \sigma_{xx} \\ \sigma_{yy} \\ \sigma_{zz} \\ \sigma_{yz} \\ \sigma_{xz} \\ \sigma_{xy} \end{pmatrix}, \tag{A8}$$

where

$$S_{66} = 2\,(S_{11} - S_{12}). \tag{A9}$$

The shape of the tensor for the cubic symmetry (in both Si(100) and Si(110)) is the same as for the hexagonal one. The subsequent treatment is valid for the cubic symmetry with $S_{66} = S_{44}$ and $S_{13} = S_{12}$.

According to WJB, it is useful now to have the jumps in displacements occur over a surface which is perpendicular to the free surface instead of across the slip plane. All quantities in the substrate have a $*$ superscript to distinguish them from quantities related to the thin film. The Fourier transform (FT)

of a function f is denoted by f^{FT}. It is possible to split the problem into two independent parts, resolving the edge and the screw components separately.

A.1. *Edge component*

The displacement field in the thin film can be decomposed into

$$\boldsymbol{u} = \frac{1}{2}\boldsymbol{b_e}\mathrm{sgn}(x) + \boldsymbol{v}, \tag{A10}$$

where $\boldsymbol{b_e} = (b_x, 0, b_z)$ and the function $\boldsymbol{v}$ is continuous for all x. The strain field (and thus also the stress field) inside the thin layer is determined only by the $\boldsymbol{v}$ part as (except at the cut surface $x = 0$) the derivatives of the sgn(x) function are equal to zero everywhere. To solve this problem, the Fourier-transformed variables are employed:

$$f^{FT}(\xi, z) = \frac{1}{\sqrt{2\pi}} \int_{-\infty}^{\infty} \mathrm{e}^{i\xi x} f(x, z) dx. \tag{A11}$$

The Fourier transform of the $\partial/\partial x$ operator is $-i\xi$. Using (A10) and (A5), the Fourier components of the strain tensor are:

$$\epsilon_{xx}^{FT}(\xi, z) = -i\xi v_x^{FT}(\xi, z), \tag{A12a}$$

$$\epsilon_{zz}^{FT}(\xi, z) = \frac{\partial v_z^{FT}}{\partial z}(\xi, z), \tag{A12b}$$

$$\epsilon_{xz}^{FT}(\xi, z) = \frac{1}{2}\left(\frac{\partial v_x^{FT}}{\partial z}(\xi, z) - i\xi v_z^{FT}(\xi, z)\right). \tag{A12c}$$

The equilibrium conditions [5] take the form

$$\frac{\partial \sigma_{xx}}{\partial x} + \frac{\partial \sigma_{xz}}{\partial z} = 0, \tag{A13a}$$

$$\frac{\partial \sigma_{xz}}{\partial x} + \frac{\partial \sigma_{zz}}{\partial z} = 0. \tag{A13b}$$

Transforming these equations into their Fourier equivalents and using Hooke's law with the stiffness tensor gives the system of partial differential equations for the FT components of the displacements v_x^{FT} and v_z^{FT}:

$$\begin{pmatrix} -C_{11}\xi^2 + C_{44}\dfrac{\partial^2}{\partial z^2} & -i\xi\,(C_{13} + C_{44})\dfrac{\partial}{\partial z} \\ -i\xi\,(C_{13} + C_{44})\dfrac{\partial}{\partial z} & -C_{44}\xi^2 + C_{33}\dfrac{\partial^2}{\partial z^2} \end{pmatrix} \begin{pmatrix} v_x^{FT} \\ v_z^{FT} \end{pmatrix} = \begin{pmatrix} 0 \\ 0 \end{pmatrix}. \tag{A14}$$

In order to simplify the notation, the quantities $A = -C_{11}$, $B = C_{44}$, $C = -i(C_{13} + C_{44})$, $D = -C_{44}$ and $E = C_{33}$ are introduced. From the second equation of the system, one obtains

$$\xi C\frac{\partial v_x^{FT}}{\partial z} = -D\xi^2 v_z^{FT} - E\frac{\partial^2 v_z^{FT}}{\partial z^2}. \tag{A15}$$

Using this equation and its twice-differentiated form with respect to z and substituting them into the first equation of the system (A14), which is once differentiated with respect to z, yields

$$EB\frac{\partial^4 v_z^{FT}}{\partial z^4} + \left(EA + DB - C^2\right)\xi^2\frac{\partial^2 v_z^{FT}}{\partial z^2} + AD\xi^4 v_z^{FT} = 0. \tag{A16}$$

We are looking for a solution of the exponential form $e^{\lambda|\xi|z}$. The proper λs are solutions of the characteristic equation

$$EB\lambda^4 + \left(EA + DB - C^2\right)\lambda^2 + AD = 0. \tag{A17}$$

Solutions are $\lambda_1 = \kappa_1$, $\lambda_2 = -\kappa_1$, $\lambda_3 = \kappa_2$ and $\lambda_4 = \kappa_2$, where

$$\kappa_{1,2} = \sqrt{\frac{-\left(EA + DB - C^2\right) \pm \sqrt{\left(EA + DB - C^2\right)^2 - 4ABDE}}{2EB}}. \tag{A18}$$

Therefore, the general solution to (A16) has the form [5]

$$v_z^{FT} = \sum_{i=1}^{4} A_i \lambda_i \, |\xi| \, e^{\lambda_i |\xi| z}, \tag{A19}$$

where A_i are functions of ξ to be determined. The component v_x^{FT} can then be obtained from (A15). Its general solution is

$$v_x^{FT} = -\sum_{i=1}^{4} A_i \xi \frac{D + E\lambda_i^2}{C} e^{\lambda_i |\xi| z}. \tag{A20}$$

Evidently,

$$\frac{D + E\lambda_i^2}{C} = -i \frac{C_{44} - C_{33}\lambda_i^2}{C_{13} + C_{44}}. \tag{A21}$$

The FT components of the strain tensor are now easy to obtain from combining Equations (A19), (A20) and (A12):

$$\varepsilon_{xx}^{FT} = \sum_{i=1}^{4} A_i \xi^2 \frac{C_{44} - C_{33}\lambda_i^2}{C_{13} + C_{44}} e^{\lambda_i |\xi| z}, \tag{A22a}$$

$$\varepsilon_{xz}^{FT} = -\frac{1}{2} \sum_{i=1}^{4} i A_i \, |\xi| \, \xi \lambda_i \frac{C_{13} + C_{33}\lambda_i^2}{C_{13} + C_{44}} e^{\lambda_i |\xi| z}, \tag{A22b}$$

$$\varepsilon_{zz}^{FT} = \sum_{i=1}^{4} A_i \xi^2 \lambda_i^2 e^{\lambda_i |\xi| z}. \tag{A22c}$$

Using Hooke's law, which has the same form when Fourier transformed, one obtains:

$$\sigma_{xx}^{FT} = C_{11}\varepsilon_{xx}^{FT} + C_{13}\varepsilon_{zz}^{FT} = -\sum_{i=1}^{4} A_i \xi^2 \lambda_i^2 C_{44} \frac{C_{13} + C_{33}\lambda_i^2}{C_{13} + C_{44}} e^{\lambda_i |\xi| z} \tag{A23a}$$

$$\sigma_{xz}^{FT} = 2C_{44}\varepsilon_{xz}^{FT} = -\sum_{i=1}^{4} i A_i \, |\xi| \, \xi \lambda_i C_{44} \frac{C_{13} + C_{33}\lambda_i^2}{C_{13} + C_{44}} e^{\lambda_i |\xi| z} \tag{A23b}$$

$$\sigma_{zz}^{FT} = C_{13}\varepsilon_{xx}^{FT} + C_{33}\varepsilon_{zz}^{FT} = \sum_{i=1}^{4} A_i \xi^2 C_{44} \frac{C_{13} + C_{33}\lambda_i^2}{C_{13} + C_{44}} e^{\lambda_i |\xi| z}, \tag{A23c}$$

where the identity $C_{11}C_{44} + \left(C_{13}^2 + 2C_{13}C_{44} - C_{11}C_{33}\right)\lambda_i^2 + C_{44}C_{33}\lambda_i^4 = 0$ was used in the expression for σ_{xx}^{FT}.

The general solution for the substrate region takes the same form (except that all variables have a star superscript). We assume that the substrate is not influenced by the thin layer as $z \to -\infty$. To fulfil this condition, the constants A_2^* and A_4^* must be identically zero. Boundary conditions must be employed now in order to determine the constants A_1, A_2, A_3, A_4, A_1^* and A_3^*.

The Fourier transform of $1/2\ \mathrm{sgn}(x)$ is $\mathrm{i}/\left(\sqrt{2\pi}\xi\right)$. The continuity of displacements across the interface $z = 0$ is expressed by the following equations:

$$v_x^{FT}(\xi, 0) + \frac{ib_x}{\sqrt{2\pi}\xi} = v_x^{*FT}(\xi, 0), \tag{A24a}$$

$$v_z^{FT}(\xi, 0) + \frac{ib_z}{\sqrt{2\pi}\xi} = v_z^{*FT}(\xi, 0), \tag{A24b}$$

which result in the equations

$$(A_1 + A_2)\Gamma_1 + (A_3 + A_4)\Gamma_2 + \frac{b_x}{\sqrt{2\pi}\xi^2} = A_1^*\Gamma_1^* + A_3^*\Gamma_2^*, \tag{A25a}$$

$$(A_1 - A_2)\kappa_1 + (A_3 - A_4)\kappa_2 + \frac{i\,b_z}{\sqrt{2\pi}\,|\xi|\,\xi} = A_1^*\kappa_1^* + A_3^*\kappa_2^*, \tag{A25b}$$

where the notation

$$\Gamma_i = \frac{C_{44} - C_{33}\kappa_i^2}{C_{13} + C_{44}}, \qquad \Gamma_i^* = \frac{C_{44}^* - C_{33}^*\kappa_i^{*2}}{C_{13}^* + C_{44}^*}, \qquad i = 1, 2. \tag{A26}$$

has been introduced.

The second set of equations is obtained from the requirement that tractions must be continuous across the interface $z = 0$:

$$\sigma_{xz}^{FT}(\xi, 0) = \sigma_{xz}^{*FT}(\xi, 0), \tag{A27a}$$

$$\sigma_{zz}^{FT}(\xi, 0) = \sigma_{zz}^{*FT}(\xi, 0). \tag{A27b}$$

Combining Equations (A23) and (A27) gives

$$(A_1 - A_2)\kappa_1\Lambda_1 + (A_3 - A_4)\kappa_2\Lambda_2 = A_1^*\kappa_1^*\Lambda_1^* + A_3^*\kappa_2^*\Lambda_2^* \tag{A28a}$$

$$(A_1 + A_2)\Lambda_1 + (A_3 + A_4)\Lambda_2 = A_1^*\Lambda_1^* + A_3^*\Lambda_2^*, \tag{A28b}$$

where the simplifying notation

$$\Lambda_i = \frac{C_{44}\left(C_{13} + C_{33}\kappa_i^2\right)}{C_{13} + C_{44}}, \qquad \Lambda_i^* = \frac{C_{44}^*\left(C_{13}^* + C_{33}^*\kappa_i^2\right)}{C_{13}^* + C_{44}^*}, \qquad i = 1, 2, \tag{A29}$$

has been introduced.

The last set of equations arises from the requirement that the free surface is at $z = h$.

The condition $\sigma_{xz}^{FT}(\xi, h) = 0$ is expressed as

$$\left(A_1 e^{\kappa_1|\xi|h} - A_2 e^{-\kappa_1|\xi|h}\right)\kappa_1\Lambda_1 + \left(A_3 e^{\kappa_2|\xi|h} - A_4 e^{-\kappa_2|\xi|h}\right)\kappa_2\Lambda_2 = 0 \tag{A30}$$

and the requirements $\sigma_{zz}^{FT}(\xi, h) = 0$ yield

$$\left(A_1 e^{\kappa_1|\xi|h} + A_2 e^{-\kappa_1|\xi|h}\right)\Lambda_1 + \left(A_3 e^{\kappa_2|\xi|h} - A_4 e^{-\kappa_2|\xi|h}\right)\Lambda_2 = 0. \tag{A31}$$

Equations (A25), (A28), (A30) and (A31) constitute a linear system of equations for the unknown variables $A_1, \ldots, A_3^*$. Obviously, the solution of this system provides $A_1, \ldots, A_3^*$ as the functions of ξ. To obtain the stress components σ_{xx}, σ_{xz} and σ_{zz}, it is necessary to perform the inverse Fourier transforms of σ_{xx}^{FT}, σ_{xz}^{FT} and σ_{zz}^{FT}, respectively, with the substituted resolved constants $A_1, \ldots, A_4$.

An attempt to obtain an analytical formula for the stress components and energy for the edge type dislocation would be unreasonably complicated and would not give any direct insight. Therefore, the calculations were performed numerically.

A.2. *Screw component*

The procedure for the screw component is similar, but simpler. The Burgers vector of a screw dislocation has only one non-zero component, b_y, and thus the only non-zero component of the displacement is u_y. Moreover, it is again a plane strain problem, i.e. $\partial/\partial y = 0$. As a consequence, the only non-zero strain components are ε_{xy} and ε_{yz}. Similar to the case of the edge dislocation, it is more convenient to deal with the FT component u_y^{FT}, rather than with u_y itself. The FT components of the strain are

$$\varepsilon_{xy}^{FT} = -\frac{1}{2} i\xi v_y^{FT}, \tag{A32a}$$

$$\varepsilon_{yz}^{FT} = \frac{1}{2} \frac{\partial v_y^{FT}}{\partial z}, \tag{A32b}$$

and the FT stress components obtained from Hooke's law are

$$\sigma_{xy}^{FT} = 2C_{66}\varepsilon_{xy}^{FT} = -i\xi C_{66} v_y^{FT}, \tag{A33a}$$

$$\sigma_{yz}^{FT} = 2C_{44}\varepsilon_{yz}^{FT} = C_{44} \frac{\partial v_y^{FT}}{\partial z}. \tag{A33b}$$

The equilibrium condition [5]

$$\frac{\partial \sigma_{xy}}{\partial x} + \frac{\partial \sigma_{yz}}{\partial z} = 0 \tag{A34}$$

provides the second-order differential equation for v_y^{FT}:

$$-\xi^2 C_{66} v_y^{FT}(\xi, z) + C_{44} \frac{\partial^2 v_y^{FT}}{\partial z^2}(\xi, z) = 0, \tag{A35}$$

the general solution of which is

$$v_y^{FT} = A_1 \mathrm{e}^{\sqrt{\frac{C_{66}}{C_{44}}}|\xi| z} + A_2 \mathrm{e}^{-\sqrt{\frac{C_{66}}{C_{44}}}|\xi| z}. \tag{A36}$$

The general solution in the substrate has exactly the same form except for the fact that all variables have a superscript. $A_2^* = 0$ because one requires all quantities to vanish as $z \to -\infty$. Applying the same boundary conditions as in the case of the edge dislocation (continuity of displacements and tractions over the interface $z = 0$ and the free surface at $z = h$) yields

$$A_1 + A_2 + \frac{i b_y}{\sqrt{2\pi}\xi} = A_1^*, \tag{A37a}$$

$$(A_1 - A_2)\sqrt{C_{66}C_{44}} = A_1^* \sqrt{C_{66}^* C_{44}^*}, \tag{A37b}$$

$$A_1 \mathrm{e}^{\sqrt{\frac{C_{66}}{C_{44}}}|\xi| h} - A_2 \mathrm{e}^{-\sqrt{\frac{C_{66}}{C_{44}}}|\xi| h} = 0. \tag{A37c}$$

Values of A_1 and A_2 fulfilling these equations are

$$A_1 = \frac{i b_y}{\sqrt{2\pi}\xi} \frac{\sqrt{C_{66}^* C_{44}^*}\, \mathrm{e}^{-2\sqrt{\frac{C_{66}}{C_{44}}}|\xi| h}}{\mathrm{e}^{-2\sqrt{\frac{C_{66}}{C_{44}}}|\xi| h} \left(\sqrt{C_{66}C_{44}} - \sqrt{C_{66}^* C_{44}^*}\right) - \left(\sqrt{C_{66}C_{44}} + \sqrt{C_{66}^* C_{44}^*}\right)}, \tag{A38a}$$

$$A_2 = \frac{ib_y}{\sqrt{2\pi}\xi} \frac{\sqrt{C_{66}^* C_{44}^*}}{e^{-2\sqrt{\frac{C_{66}}{C_{44}}}|\xi|h} \left(\sqrt{C_{66}C_{44}} - \sqrt{C_{66}^* C_{44}^*}\right) - \left(\sqrt{C_{66}C_{44}} + \sqrt{C_{66}^* C_{44}^*}\right)}. \quad \text{(A38b)}$$

The stress components can be obtained by the inverse Fourier transform of σ_{xy}^{FT} and σ_{xz}^{FT} with the substituted A_1 and A_2 from the last two equations.

After that, the components of the stress and the Burgers vector can be substituted in (A3) to calculate the dislocation energy.

Appendix 2. Constants of GaN, AlN, InN, Si and Ge

Table B1. The stiffness constants (in GPa) are taken from [27] for GaN, AlN and InN, from [28] for Si and from [3] for Ge. The stiffness constants of $Al_xGa_{1-x}N$/GaN, $In_xGa_{1-x}N$/GaN and $Si_{1-x}Ge_x$/Si are calculated using Vegard's law with the data in the table.

	C_{11}	C_{12}	C_{13}	C_{33}	C_{44}	C_{66}
GaN	374.2	141.4	98.1	388.6	98.3	$(C_{11}-C_{12})/2$
AlN	410.5	148.5	98.9	388.5	124.6	$(C_{11}-C_{12})/2$
InN	223	115	92	224	48	$(C_{11}-C_{12})/2$
Si(111)	194.25	35.25	63.9	165.6	79.5	50.85
Ge(111)	155	21.6	48.2	128.4	66.7	40.1

Table B2. The lattice constants (in Å) are taken from [29] for GaN, AlN and InN, from [3] for Si and Ge. The lattice constants of $Al_xGa_{1-x}N$/GaN, $In_xGa_{1-x}N$/GaN and $Si_{1-x}Ge_x$/Si are calculated using Vegard's law with the data in the table.

	GaN	AlN	InN	Si(111)	Ge(111)
a	3.22	3.11	3.54	5.43	5.65
c	5.19	4.98	5.96		

Table B3. Characteristics of the two slip systems for the wurtzite crystal structures showing the Burgers vector b, the angle ϕ between the slip plane and the normal to the substrate–film interface and the angle θ between the dislocation line and the Burgers vector. x is the Al or In content.

	b	ϕ	θ
$\frac{1}{3}\langle 1\,1\,\bar{2}\,3\rangle\{1\,1\,\bar{2}\,2\}$	$\sqrt{a^2(x)+c^2(x)}$	$\arctan\frac{a(x)}{c(x)}$	90°
$\frac{1}{3}\langle 1\,1\,\bar{2}\,3\rangle\{1\,\bar{1}\,0\,1\}$	$\sqrt{a^2(x)+c^2(x)}$	$\arctan\frac{\sqrt{3}a(x)}{2c(x)}$	$\arccos\frac{a(x)}{2b(x)}$

Table B4. Characteristics of the slip system for the diamond crystal structure $Si_{1-x}Ge_x$/Si showing the Burgers vector b, the angle ϕ between the slip plane and the normal to the substrate–film interface and the angle θ between the dislocation line and the Burgers vector. x is the Ge content.

	b	ϕ	θ
$\langle 1\,1\,0\rangle\{1\,1\,1\}$	$\sqrt{2}a(x)$	$\arctan\frac{1}{\sqrt{2}}$	60°

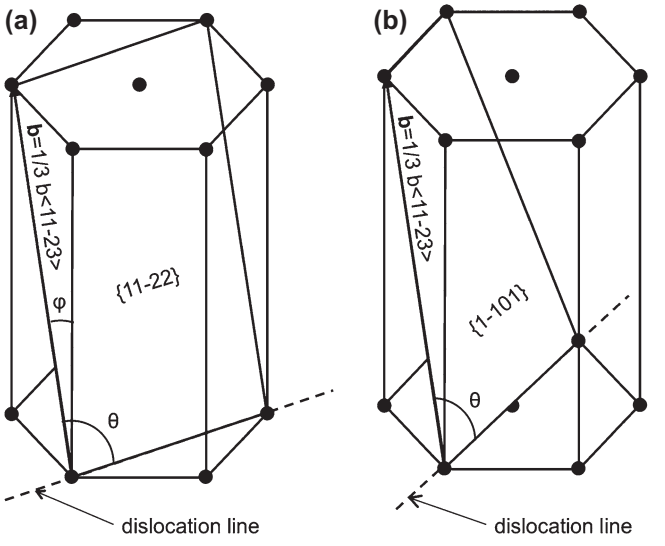

Figure B1. The two most favourable slip systems in the wurtzite systems $Al_xGa_{1-x}N$/GaN, $In_xGa_{1-x}N$/GaN: a) $\langle 1\,1\,\bar{2}\,3\rangle\{1\,1\,\bar{2}\,2\}$ observed by Srinivasan [21], and b) $\langle 1\,1\,\bar{2}\,3\rangle\{1\,\bar{1}\,0\,1\}$ determined by Jahnen [23].

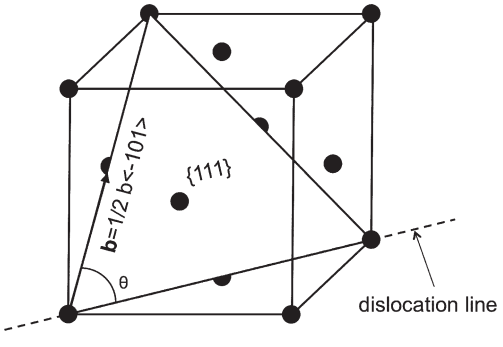

Figure B2. The slip system $\langle 1\,1\,0\rangle\{1\,1\,1\}$ of the 60° dislocation shown in the FCC structure.